Journal of the Mechanics and Physics of Solids 106 (2017) 1–14

Contents lists available at ScienceDirect

Journal of the Mechanics and Physics of Solids

journal homepage: www.elsevier.com/locate/jmps

Statistical model of rough surface contact accounting for size-dependent plasticity and asperity interaction

H. Song[a], A.I. Vakis[b], X. Liu[c], E. Van der Giessen[a,*]

[a] Department of Applied Physics, Zernike Institute for Advanced Materials, University of Groningen, Groningen 9747 AG, The Netherlands
[b] Advanced Production Engineering, Engineering and Technology Institute Groningen, University of Groningen, Groningen 9747 AG, The Netherlands
[c] State Key Laboratory of Nonlinear Mechanics, Institute of Mechanics, Chinese Academy of Sciences, Beijing 100190, PR China

ARTICLE INFO

Article history:
Received 2 February 2017
Revised 11 May 2017
Accepted 25 May 2017
Available online 26 May 2017

ABSTRACT

The work by Greenwood and Williamson (GW) has initiated a simple but effective method of contact mechanics: statistical modeling based on the mechanical response of a single asperity. Two main assumptions of the original GW model are that the asperity response is purely elastic and that there is no interaction between asperities. However, as asperities lie on a continuous substrate, the deformation of one asperity will change the height of all other asperities through deformation of the substrate and will thus influence subsequent contact evolution. Moreover, a high asperity contact pressure will result in plasticity, which below tens of microns is size dependent, with smaller being harder. In this paper, the asperity interaction effect is taken into account through substrate deformation, while a size-dependent plasticity model is adopted for individual asperities. The intrinsic length in the strain gradient plasticity (SGP) theory is obtained by fitting to two-dimensional discrete dislocation plasticity simulations of the flattening of a single asperity. By utilizing the single asperity response in three dimensions and taking asperity interaction into account, a statistical calculation of rough surface contact is performed. The effectiveness of the statistical model is addressed by comparison with full-detail finite element simulations of rough surface contact using SGP. Throughout the paper, our focus is on the difference of contact predictions based on size-dependent plasticity as compared to conventional size-independent plasticity.

1. Introduction

The roughness of practical surfaces leads to the real contact area being only a small portion of the apparent contact area. The friction force is usually written as $F_f = \mu F_n$, where μ is the friction coefficient and F_n is the normal force, but it can also be interpreted as $F_f = \tau A$ with τ being the contact interfacial shear strength and A being the real contact area. The above two types of interpretations indicate a linear relation between F_n and A, if it is assumed that both the interfacial shear strength τ and the friction coefficient μ are constants.

It is well accepted by now that the origin of the proportionality between real contact area and load resides in the random nature of the asperities on real rough surfaces. For elastic materials with a fractal surface, Persson (2001) has developed a

* Corresponding author.
E-mail address: e.van.der.giessen@rug.nl (E. Van der Giessen).

http://dx.doi.org/10.1016/j.jmps.2017.05.014
0022-5096/

theory that is exact for complete contact, i.e. at high loads. Besides being dependent on the statistical properties of the surface, the theoretical prediction of a linear relation between contact area and applied load relies on the fact that the long-range interactions between contacting asperities are incorporated. So far, Persson's theory has passed all critical tests for elastic materials, e.g., Campana et al. (2008), and has been successfully applied to study leakage of rubbers (Persson, 2001).

An earlier, seminal work on contacting rough surfaces is that by Greenwood and Williamson (1966) (GW) who proposed to represent a rough surface by a spatial distribution of hemispherical asperities with a constant radius of curvature, while the summit height of the asperities follows a Gaussian distribution. While many surfaces do exhibit fractal roughness, a description with Gaussian statistics is a well-accepted approximation of rough surfaces, see e.g. Li and Torrance (2005). Apart from the different statistics of the surface roughness, the GW model is built on numerous simplifying assumptions and therefore has limitations in comparison with Persson's theory. However, with a view on subsequent understanding of static friction on metallic surfaces at low loads, a GW approach is appealing because it is designed for small contact areas. Moreover, GW models have the simplicity that is needed for our purpose.

After its inception in 1966, several assumptions in the GW model related to the asperity tip shape have been relaxed by, notably, Bush et al. (1975), Greenwood (2006), Carbone and Bottiglione (2008) and Carbone (2009). A key difference with Persson's theory (Persson, 2001) is that the original GW model assumed that asperities deform independently from each other. This assumption greatly simplifies the calculation of the contact force F_n but ignores the fact that all asperities share the same substrate. Deformation of contacting asperities will deflect the substrate and thereby shift down all other asperities by an amount that depends on the distance to the contacting asperity and the response of the contacting asperity. Ciavarella et al. (2008) have extended the GW model to incorporate such asperity interaction over a finite surface area by treating the contact pressure as being uniformly distributed over the apparent contact area and the resulting deformation as being uniform. Chandrasekar et al. (2013) introduced asperity interaction by making use of the Hertz solution, while Vakis (2014) subsequently accounted for interaction between contacting asperities and their non-contacting neighbors through a statistical method. Song et al. (2014) re-visited the model and derived a modified theory in which the interaction effect converges with increasing order of interaction and effectively reduces the contact force compared with the analysis in which the interaction effect is absent.

Noting that the peak contact pressure in asperities in all of these GW-type models exceeds the yield strength of metals at small loads, Chang et al. (1987) introduced plasticity into the original GW model. Subsequent work by Kogut and Etsion (2002) utilized the finite element method based on J_2 plasticity theory and developed curve-fitted force-vs-deformation expressions for the contact between sphere and a rigid flat, which were then introduced into the GW model.

Since real rough surfaces have asperities at various length scales, it is important to note that plasticity of small samples of a crystalline material is size dependent below tens of microns, with smaller samples having a higher yield stress. Therefore, size-dependent plasticity needs to be taken into account in rough surface contact problems. Jackson (2006) tried to incorporate size-dependent plasticity into the GW model by direct application of the Nix-Gao relation (Nix and Gao, 1998a) for the indentation size effect. Though attractive this simple approach may be, it ignores the following fundamental issues: (i) size-dependent plasticity strongly depends on the sample geometry and there is no proof that size effects in asperity flattening are the same as in indentation; (ii) the plasticity size effect in asperity flattening cannot be fully captured by only changing the yield stress (hardness): enhancement of the flow strength by the local plastic strain gradient is different from an overall increase. The difference has been observed in Song et al. (2016) in the distribution of the contact pressure: for J_2 plasticity, a change of the material yield stress will simply shift the distribution, while size-dependent plasticity also changes the shape of the distribution.

At a more fundamental level, two-dimensional (2D) discrete dislocation plasticity (DDP) simulations have successfully captured size effects in a variety of different problems, such as bending (Cleveringa et al., 1999), indentation (Widjaja et al., 2005), and tension (Deshpande et al., 2005). Recently, the method has been applied in contact and friction studies, such as asperity flattening (Sun et al., 2012) and asperity ploughing (Song et al., 2015). The conventional mechanism-based strain gradient plasticity theory (CMSGP) is a continuum theory that has been used to describe the indentation size effect (Qu et al., 2004; Zhang et al., 2006) and the effect of particle size in composite materials (Xue et al., 2002). Recently CMSGP has been applied to 3D rough surface contact (Song et al., 2016), revealing a strong difference with the predictions by size-independent J_2 plasticity. The FEM simulations involved, however, put a high demand on computational resources and time.

The model presented in this paper is the first to incorporate both size-dependent plasticity and asperity interaction in a statistical approach to rough surface contact based on the response of individual asperities. The elastoplastic response of a single asperity under contact is characterized by strain gradient plasticity (SGP). The intrinsic length in the SGP model is fitted by comparison of DDP simulations of the flattening of idealized asperities of different size. Asperity interaction is implemented through the method in Vakis (2014) and Song et al. (2014). Finally, predictions by the statistical summation model will be compared with a full-blown FEM simulation to verify the accuracy and effectiveness of the statistical model. Throughout this work, the objective is to gain insight in the effect of the size dependence of asperity plastic deformation on the overall contact response.

2. Description of the problem

A numerically generated random rough surface, see Fig. 1, with nominal area of 10 μm × 10 μm is compressed by a rigid flat surface. Given a value for the root mean square (rms) height and surface correlation length l_s, an isotropic rough surface

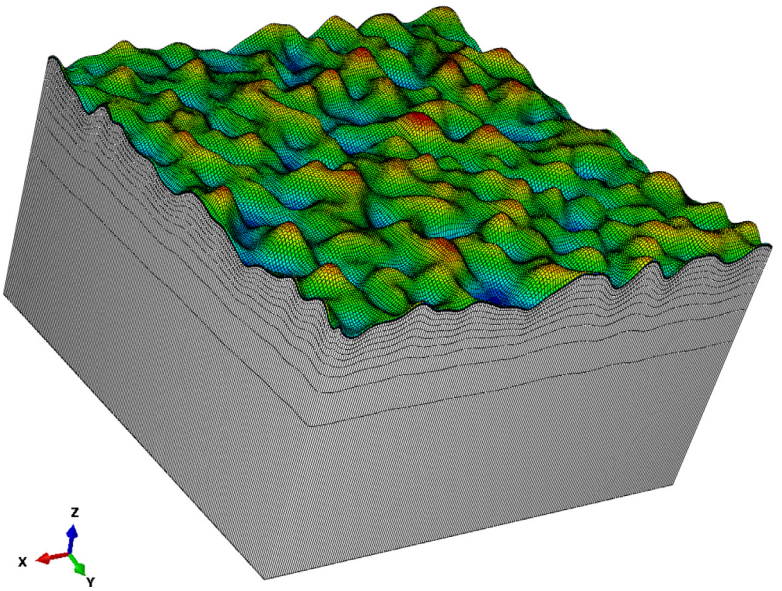

Fig. 1. Deformable rough surface on a substrate, contour color: blue—valley, red—peak. (For interpretation of the references to color in this figure legend, the reader is referred to the web version of this article.)

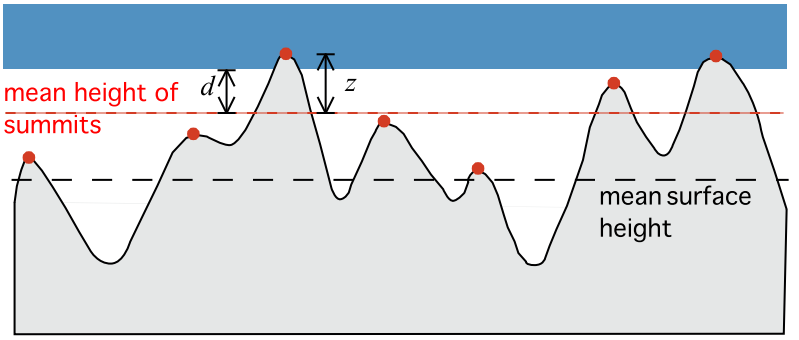

Fig. 2. Sketch of a rough surface under contact with a rigid flat indicated by the blue bar. The distance from the rigid flat to the mean summit height is d, while z is the height of a particular summit relative to the mean summit height. The asperity interference is $U = z - d$. (For interpretation of the references to color in this figure legend, the reader is referred to the web version of this article.)

with Gaussian statistics is generated by the numerical method described in Song et al. (2016). The spectral moments of the surface can be determined from the height profile (for isotropic surfaces) as in McCool (1987), i.e.,

$$m_0 = \mathrm{AVG}(z^2(x)),\ m_2 = \mathrm{AVG}[(dz(x)/dx)^2],\ m_4 = \mathrm{AVG}[(d^2z(x)/dx^2)^2]. \tag{1}$$

where AVG represents the arithmetic average and $z(x)$ indicates a 2D trace of the surface heights along an arbitrary x-direction of the 3D surface. These spectral moments define the average asperity tip curvature R, the areal asperity number density η and the standard deviation σ_s of summit heights as follows:

$$R = 0.375(\pi/m_4)^{1/2},\ \eta = (m_4/m_2)/6\pi\sqrt{3},\ \sigma_s = (1 - 0.8968/\alpha)^{1/2} m_0^{1/2}, \tag{2}$$

where $\alpha = (m_0 m_4)/m_2^2$ (McCool, 1987). With the above parameters, the contact of the numerically generated rough surface can be dealt with in a GW statistical method (Greenwood and Williamson, 1966), as illustrated in Fig. 2.

The height of the rough surface follows a normal distribution with standard deviation σ. It is assumed that the summit height also follows a Gaussian distribution, yet with a standard deviation σ_s. The difference between σ_s and σ is that the former only includes information about the asperity tips while the latter also includes information on the valleys. According to McCool (1986), σ and σ_s are related through

$$\sigma_s = \sqrt{\sigma^2 - \frac{3.717 \times 10^{-4}}{\eta^2 R^2}}\,. \tag{3}$$

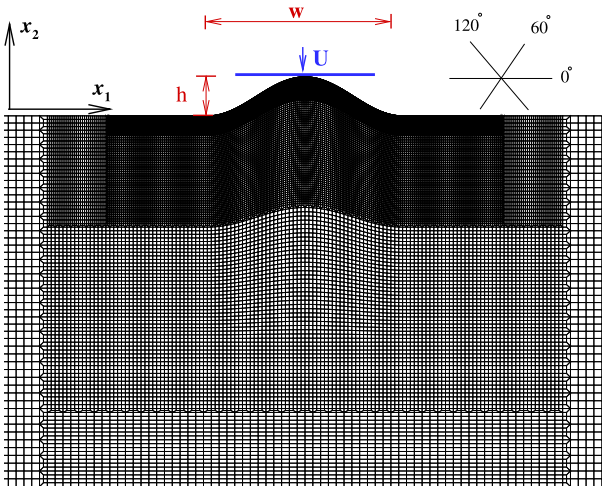

Fig. 3. Contact between a single asperity and a rigid flat in DDP calculation. Three slip systems with orientations 0°, 60° and 120° are used. The finite element is highly refined around the asperity to capture contact evolution precisely.

3. Mechanical response of a single asperity

The mechanical response of a single asperity in existing GW-type statistical models was assumed to be either purely elastic or size-independent elastoplastic. In this section, the size-dependent elastoplastic response of a single asperity in contact is characterized by conventional mechanism-based strain gradient plasticity (CMSGP). The CMSGP theory is implemented through ABAQUS user subroutine UMAT. Four-node axisymmetric full integration (CAX4) elements are used, and the plastic strain gradients are computed at Gauss points by using the differentiation of shape functions. In CMSGP, the material flow stress σ_{flow} not only depends on the equivalent plastic strain ε^{p} but also on a scalar measure, η^{p}, of the plastic strain gradient through

$$\sigma_{\text{flow}} = \sigma_{\text{Y}}\sqrt{f^2(\varepsilon^{\text{p}}) + l\eta^{\text{p}}}. \tag{4}$$

Here, σ_{Y} is the material initial yield strength, $f(\varepsilon^{\text{p}})$ describes the material strain hardening, and l is the intrinsic material length. Details of the theory can be found in Huang et al. (2003) and Zhang et al. (2006).

One of the limitations of CMSGP is that the value of l can be different under different loading conditions as l reflects the material micro-structure. Therefore, the value of l is usually determined by experiments for a specific problem; for example, l is 4 μm in torsion of copper wires (Fleck et al., 1994) while it is 12 μm for the indentation of annealed single crystal copper (Nix and Gao, 1998b). As far as we know, no asperity contact experiments have been carried out to determine the value of l. Thus, we make use of the idea of multiscale modeling in order to extract the parameter from a simulation at a smaller length scale.

3.1. Multiscale modeling of sinusoidal asperity flattening

In continuum plasticity theories, such as J_2 flow theory and strain gradient plasticity theory, plasticity is described by phenomenological parameters, such as the yield strength σ_{Y} and the strain hardening function, etc. By contrast, discrete dislocation plasticity (DDP) tracks all individual dislocations in an elastic background. Plasticity is described through the generation, motion and annihilation of dislocations, and yield strength and hardening rate are outcomes of the computation. In this section, we report on 2D sinusoidal asperity flattening simulations by DDP and CMSGP together to determine the value of l.

The model problem is shown in Fig. 3. A sinusoidal asperity with wavelength w and height h, lies on a very large substrate to exclude the finite size effect of the substrate. The asperity is compressed by a rigid flat. Discrete dislocation plasticity in the asperity is investigated within the Van der Giessen and Needleman (1995) framework, where traction and displacement boundary conditions are incorporated using superposition. The aspect ratio of the asperity is $w/h = 5$ as in Sun et al. (2012). The crystal is taken to have properties that are reminiscent of aluminum with Young's modulus $E = 70$ GPa and Poisson's ratio $\nu = 0.33$. Three slip systems are used whose orientations (0°, 60° and 120°) are indicated in Fig. 3. The slip planes are spaced at $200b$, where b is the Burgers vector magnitude of 0.25 nm. Dislocation sources and obstacles are randomly distributed over the slip planes with densities of 60 μm^{-2} and 120 μm^{-2} respectively. The sources mimic the Frank-Read mechanism of dislocation generation in 2D, and are characterized by a strength and the time needed to generate a new dipole (Van der Giessen and Needleman, 1995). The strength of the sources to generate edge dislocations is selected randomly from a Gaussian distribution with mean value $\bar{\tau}_{\text{nuc}} = 50$ MPa, and 20% (10 MPa) standard deviation. The strength

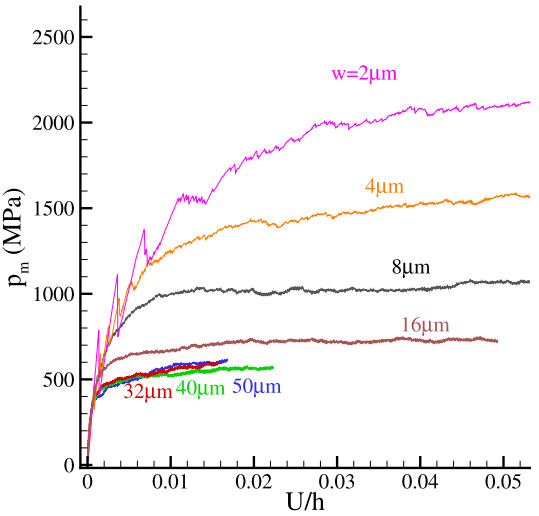

Fig. 4. Mean contact pressure versus asperity strain for different sizes of asperity carried out by DDP.

of the obstacles, τ_{obs}, is taken to be 200 MPa. We assume the same loading rate $\dot{U}$ of 0.04 nm/ns as in earlier asperity studies (Song et al., 2015; Sun et al., 2012). Since source strength and position, as well as obstacle position are randomly distributed, each case is repeated for 10 different realizations of strength and position to average out stochastic variations.

The mean contact pressure p_m is defined as

$$p_{\mathrm{m}} = 1/C \int p(x_1)dx_1,\ x_1 \in C \tag{5}$$

where C is the contact area between the rigid flat and sinusoidal asperity. The contact area gradually evolves with increased flattening displacement U which is imposed as a prescribed vertical displacement. We also define a strain-like measure for the asperity $\varepsilon_{asp} = U/h$.

It can be seen in Fig. 4 that when the asperity size $w < 32$ μm, there is a strong size effect with smaller asperities having higher mean contact pressure at the same asperity strain.

When $w \geq$ 32 μm, the DDP results become size independent and therefore should also be captured by J_2 plasticity. For J_2 plasticity theory, we assume exponential hardening in the form

$$\sigma = \sigma_{\mathrm{Y}}\left(1 + \frac{E\varepsilon^{\mathrm{p}}}{\sigma_{\mathrm{Y}}}\right)^{n}, \tag{6}$$

where n is the hardening exponent. First, by looking at the point where the DDP result starts to deviate from the result of the purely elastic model of asperity flattening, we determine the initial yield strength σ_Y in the J_2 model. Then, with this value of σ_Y, the hardening exponent n can be determined by fitting the rest of the DDP result.

Fig. 5 shows that the DDP prediction with dislocation properties specified by $\rho_{nuc} = 60\ \mu m^{-2}$, $\rho_{obs} = 120\ \mu m^{-2}$, $\bar{\tau}_{nuc} =$ 50 MPa, and $\tau_{obs} = 200$ MPa is accurately captured by J_2 theory with an initial yield strength $\sigma_Y = 210$ MPa and hardening exponent $n = 0.1$.

Turning now to the smaller asperities with $w < 32$ μm, Fig. 6 shows that their size-dependent response as predicted by DDP can be captured by the CMSGP model when the intrinsic length l is taken as 4.4 μm. This is similar to the intrinsic length ($\sim$ 5 μm) obtained from indentation experiments of aluminum (Fuguo et al., 2014). The reason for the increasing deviation between DDP and CMSGP results for smaller asperities in the small strain regime (Fig. 6(b) versus (a)) is that when the asperity becomes smaller, the early stage of DDP is dislocation source limited, whereas the SGP model is a continuum theory implying unrestricted availability of dislocation sources.

3.2. Parameterized single-asperity response

In order to relax the limitation to elastic asperities in the original GW model, Kogut and Etsion (2002) carried out FEM simulations of the flattening of a half sphere using J_2 plasticity and parameterized the elastoplastic response (contact force and contact area) as a function of asperity interference. Their results have been used in several subsequent elastoplastic extensions of GW type statistical models, such as Chandrasekar et al. (2013) and Vakis (2014). Following Kogut and Etsion (2002), in this section, we propose a parameterized function for a single asperity response that takes size-dependent plasticity into account.

The model problem is the same as that in Kogut and Etsion (2002): a hemisphere with radius R is compressed by a rigid flat, see Fig. 7. The contact between rigid flat and sphere is frictionless. Based on the ball indentation hardness test of Tabor

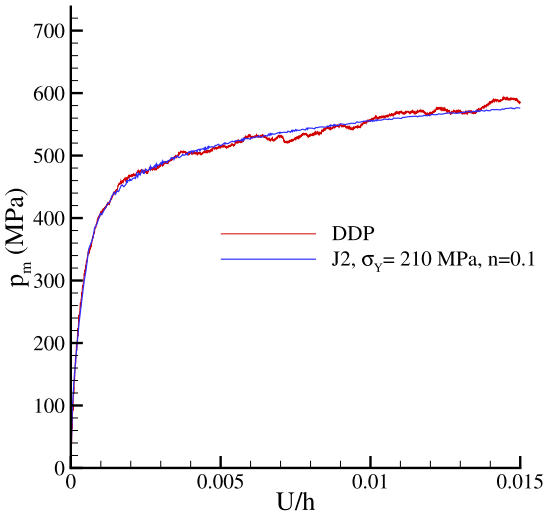

Fig. 5. Comparison between DDP and J_2 plasticity: mean contact pressure versus asperity strain for the asperity size $w = 32\mu$m.

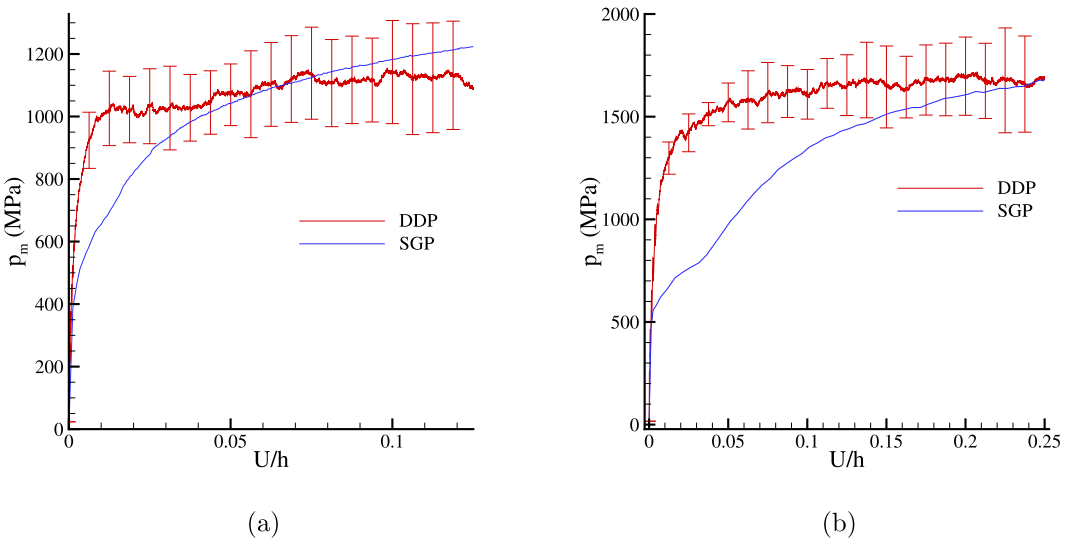

Fig. 6. Comparison between DDP and SGP plasticity: mean contact pressure versus asperity strain for the asperity size (a) $w = 8$ μm, (b) $w = 4$ μm.

(2000), Greenwood and Williamson estimated that the limit of elastic deformation (Greenwood and Williamson, 1966) is reached when the maximum Hertz pressure is about 60% of the material hardness H. Kogut and Etsion (2002) adopted the results of (Chang et al., 1987) in which the maximum contact pressure at the inception of plastic deformation is generalized as KH, where K is a coefficient defined as $K = 0.454 + 0.41\nu$ and $H = 2.8\sigma_Y$. Therefore, the critical interference U_c that marks the transition from purely elastic to elastoplastic deformation is given by

$$U_c = \left(\frac{\pi KH}{2E}\right)^2 R. \tag{7}$$

The corresponding critical contact force and contact area are

$$F_c = \frac{2}{3}KH\pi RU_c\,, \quad A_c = \pi RU_c\,,$$

respectively. Kogut and Etsion (2002) subdivided the entire elastoplastic response into four regimes and parameterized their FEM results for contact force F and contact area A as functions of the interference in each regime through a power law:

$$F/F_c = b(U/U_c)^m\,, \quad A/A_c = c(U/U_c)^n. \tag{8}$$

where constants b, m, c, n are fit parameters.

In this work, we parameterize the asperity response with different material's plastic properties that are obtained in the previous section (J_2 with strain hardening, SGP model). The elasto-perfectly plastic model which is used in the original

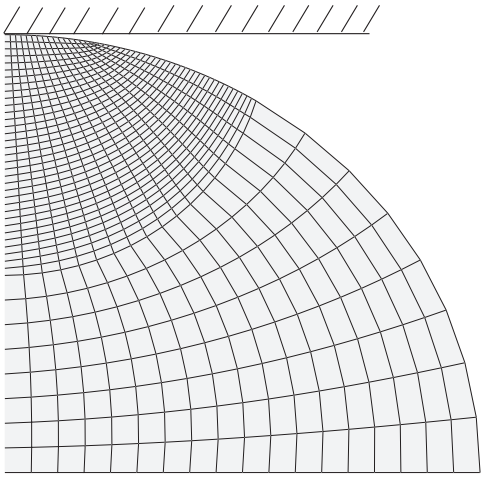

Fig. 7. Axisymmetric model to study the contact between a hemispherical dome and a rigid flat. The mesh used in the actual simulations is eight times finer than that shown here for clarity.

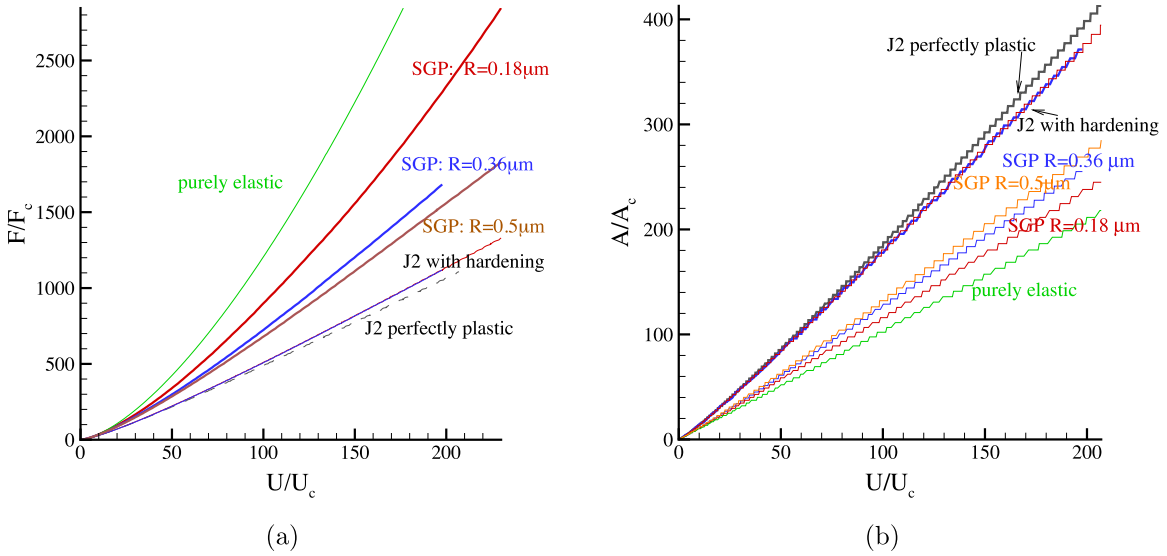

Fig. 8. Response of a hemispherical asperity: (a) Dimensionless force versus dimensionless interference, (b) dimensionless contact area versus dimensionless interference. The jaggedness of the contact area is a numerical artifact of tracing nodes in contact: the contact area increases by at least the length of an element. Since the elements gradually become larger away from the summit of the asperity, the jumps in contact length grow as the contact increases.

Kogut–Etsion (KE) model (Kogut and Etsion, 2002) is also utilized to highlight the difference between different plasticity models. Just like in Kogut and Etsion (2002), the asperity response is subdivided into four regimes; the values of the fit parameters b_i, m_i, c_i, n_i in Eq. (8) for the different models are summarized in Table 3, see Appendix. Fig. 8a shows the normalized force-interference response for a few typical values of R that appear in the numerically generated random surfaces with different roughness. In contrast to J_2 plasticity, predictions by SGP reveal the typical size effect: smaller is harder. Consistent with this, Fig. 8b shows that compared with J_2 plasticity, size-dependent plasticity yields a smaller contact area. For contact force as well as contact area, the effect of hardening (with hardening exponent $n = 0.1$) in J_2 plasticity is quite small.

4. Statistical analysis of rough surface contact

After having characterized the mechanical response of a single asperity in contact, we use this single asperity response in a rough surface contact analysis. For this, it is assumed that the summit height follows a Gaussian distribution with standard deviation σ_s. Following Kogut and Etsion (2002), all length dimensions are normalized by the standard deviation of the surface height distribution σ. Denoting non-dimensionalized quantities with a superscript *, the probability density

function of summit heights takes the form

$$\varphi^*(z^*) = \frac{1}{\sqrt{2\pi}}\left(\frac{\sigma}{\sigma_s}\right)\exp\left[-\frac{1}{2}\left(\frac{\sigma}{\sigma_s}\right)^2 (z^*)^2\right].$$

Thus, for a surface with nominal contact area A_n and asperity density η, the number of asperities in contact is

$$N_c = \eta A_n \int_{d^*}^{\infty} \varphi^*(z^*)\mathrm{d}z^*.$$

Knowing the mechanical response of a single asperity as a function of the local interference, $F(z-d)$, we can determine the total force on the whole rough surface by summing all individual asperity contributions. The total contact force on the surface can then be written as

$$F_{\mathrm{sum}} = \eta A_n \int_d^{\infty} F(z-d)\varphi(z)\mathrm{d}z,$$

while the real contact area of the surface becomes

$$A_{\mathrm{real}} = \eta A_n \int_d^{\infty} A(z-d)\varphi(z)\mathrm{d}z.$$

After normalization by the hardness H and insertion of the Kogut–Etsion relations (7) and (8), the nominal contact pressure, defined as $F^* = F_{\mathrm{sum}}/A_{\mathrm{n}}$, for the whole surface takes the form

$$F^* = \frac{F_{\mathrm{sum}}}{A_{\mathrm{n}}H} = \frac{2}{3}\pi\beta K U_c^* \int_{d^*}^{\infty} b\left(\frac{z^*-d^*}{U_c^*}\right)^m \varphi^*(z^*)dz^* \tag{9}$$

where $\beta = \sigma R\eta$. We remind the reader that b and m take different values for different regimes of the power-law fit in Eq. (8), see Appendix. This means that, in practice, the integral needs to be split into four parts.

In the original KE model (Kogut and Etsion, 2002), the material is assumed to be perfectly plastic and the material hardness is defined as $H = 2.8\sigma_{\mathrm{Y}}$. When the material exhibits strain hardening, H is not a constant; moreover, when strain gradients are considered, H becomes size dependent. Henceforth, one might argue to just normalize stress by the initial yield strength σ_{Y}. Here however, we still use $H = 2.8\sigma_{\mathrm{Y}}$ to nondimensionalize the nominal contact pressure in keeping with the original KE model.

Similar to Eq. (9), the ratio of the real contact area to the nominal contact area, A^*, can be calculated as

$$A^* = \frac{A_{\mathrm{real}}}{A_{\mathrm{n}}} = \pi\beta U_c^* \int_{d^*}^{\infty} c\left(\frac{z^*-d^*}{U_c^*}\right)^n \varphi^*(z^*)dz^*. \tag{10}$$

Asperity interaction is incorporated by making use of the Hertz displacement field caused by an indenter of radius R in an elastic medium (Vakis, 2014). The effective shifting down Ω of the mean summit height as a function of distance from the contacting asperity changes the summit height distribution into

$$\varphi^*(z^*) = \frac{1}{\sqrt{2\pi}}\left(\frac{\sigma}{\sigma_s}\right)\exp\left[-\frac{1}{2}\left(\frac{\sigma}{\sigma_s}\right)^2 (z^* + \Omega^*(d^*))^2\right].$$

As the numerically generated rough surface has a finite surface area, the order of interaction is $n_{\max} = \sqrt{A_n\eta} - 1$. Details of asperity interaction formulations can be found in Vakis (2014) and Song et al. (2014).

As pointed out in Section 2, given a rough surface with two roughness parameters (rms and correlation length l_s), such as the one shown in Fig. 1, the GW parameters (R, η, σ_s) can be obtained from the spectral moments. For two generated surfaces of different roughness, the GW parameters are listed in the following table.

The predictions by the statistical model for different material properties are shown in Fig. 9. We observe that the predictions by J_2 theory, especially in the absence of hardening, is quite insensitive to surface roughness. This is consistent with the findings in Song et al. (2016) and Pei et al. (2005). It can be seen in Fig. 9(a) that strain hardening results in a larger contact force compared to perfect plasticity; when strain gradient plasticity is considered, the contact force is even larger. For the roughest surface considered, the prediction of SGP deviates substantially from the predictions of J_2 plasticity. For the SGP computation for a surface with roughness rms = 0.08 μm, the inset shows that interaction effect reduces the contact force compared with the case when asperity interaction is absent (shown in symbols).

Despite the mentioned variations in the force response, Fig. 9(b) reveals a roughly linear relationship between the dimensionless contact area and dimensionless contact force for different plastic models and surface roughness. We emphasize, however, that F^*/A^* is only approximately a constant. It is known that this ratio in GW-type models is not strictly constant, even in elastic contact (Carbone and Bottiglione, 2008), while in Fig. 9(b) we observe similar deviations in the case of elasto-plastic contacts. The effect is largest in the SGP model showing an increase of up to +20% relative to the initial slope at the highest loads considered here. These relatively large deviations reflect the deformation-induced nonlinear hardening in strain gradient plasticity. Asperity interaction effectively shifts the mean summit height and delays contact, but it does not

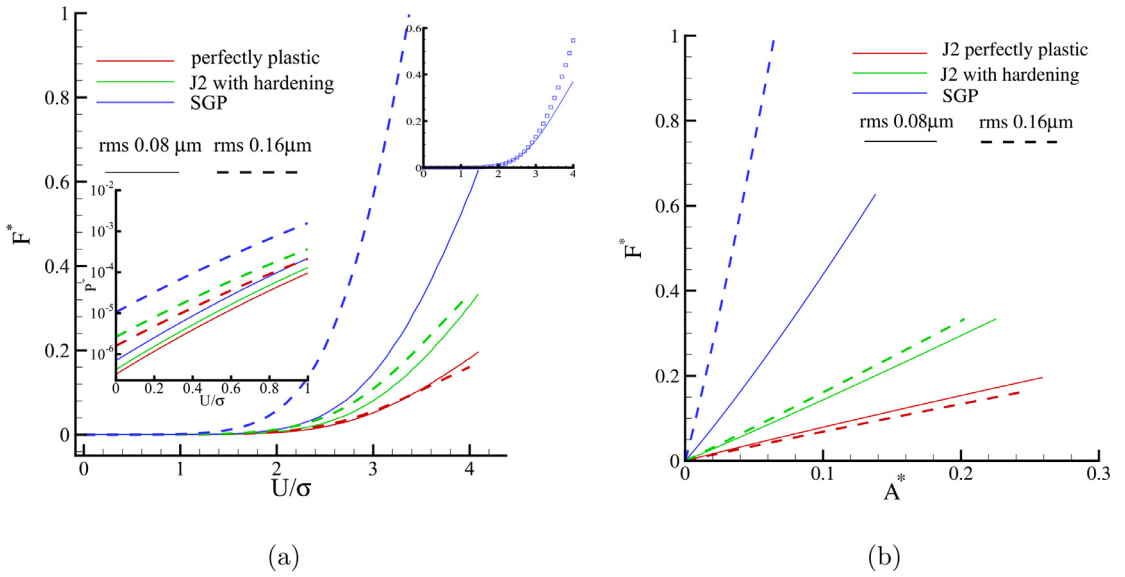

Fig. 9. Predictions by statistical model for the rough surface with roughness parameters rms = 0.08 μm, $l_s = 0.4$ μm (solid line) and rms = 0.16 μm, $l_s = 0.4$ μm (dashed line). (a) Dimensionless force versus dimensionless interference (force on a log scale is shown in the left-hand inset). The top right-hand inset shows the response with (solid line) and without (symbols) asperity interaction. (b) Dimensionless force versus dimensionless contact area.

influence the relationship between contact force and contact area. Moreover, after noting that the slope indicates the dimensionless mean contact pressure, it bears emphasis that the mean contact pressure in the SGP model is much larger than according to J_2 models.

5. Comparison between FEM predictions and statistical model

The statistical model makes several assumptions. In order to verify that the roughness-dependent influence of size-dependent plasticity presented in the previous section is not an artifact, we now compare the results with full-blown FEM computations for random rough surfaces. Details of the FEM simulation can be found in Song et al. (2016). For a given set of roughness parameters {rms, l_s}, numerical generation of random rough surfaces yields different realizations; for each group of roughness parameters, we therefore perform five simulations to average out this stochasticity.

For a rough surface characterized by rms = 0.08 μm and $l_s = 0.4$ μm, Fig. 10(a) shows a clear difference between the averaged contact forces according to the SGP and J_2 models. However, the FEM computations also reveal that the contact force is very sensitive to the randomness of the surface topography, with the standard deviation increasing with continued flattening. The contact area evolution shows a similar sensitivity, see Fig. 10(b), with the average contact area obtained from five FEM predictions with the SGP model being significantly larger than the statistical prediction.

By contrast, Fig. 10(c) reveals that the mean contact pressure F^*/A^* is not sensitive to the randomness of the surface topography as indicated by all plotted data points. This demonstrates that the near-linear relation between F^* and A^* is robust for any material model: it is the mean slope of F^* vs A^* that depends on the material properties. The qualitative trend that the mean contact pressure found in the SGP model is higher than with J_2 hardening which in turn is higher than for perfect plasticity is consistent with those according to the statistical model, but the differences are smaller.

A similar material-dependent ordering can be seen in the contact force and contact area, Fig. 10(a and b), but due to the large stochastic spread between the five realizations, these differences are not quantitatively significant, while the differences in mean contact pressure are. These observations get amplified when the rms of the surface is twice as large. In fact, according to Fig. 11(a), the statistical prediction for SGP is no longer contained in the standard deviation of the FEM results. According to Fig. 11(b), also the deviation between statistical and FEM predictions of the true mean contact pressure increases with increasing surface roughness.

In search of an explanation for this mismatch, we observed that the results of the statistical analysis in Fig. 9 are not very sensitive to the surface roughness parameters when using J_2 plasticity, but are quite sensitive for the SGP model. This is not surprising when noting then that the strain-gradient dependence in the SGP model should make it more sensitive to the curvature of the asperity tips. These observations suggest that the spectral moments analysis of GW parameters, cf. Eq (2), may underestimate R. Indeed, Refs. Kalin et al. (2016), Pawlus et al. (2012) and Yu and Polycarpou (2004) point out that the spectral moments analysis tends to yield a smaller value of R than a deterministic analysis. Therefore, we re-estimated R for the two numerically generated rough surfaces using the classical definition of the radius of curvature of the height profile $z(x)$, $R = (1 + (dz/dx)^2)^{3/2}/(d^2z/dx^2)$. It is found that $R = 0.5$ μm and 0.36 μm for the surface with rms = 0.08 μm and rms = 0.16 μm, respectively; these values are significantly smaller than those listed in Table 1 and used previously. The

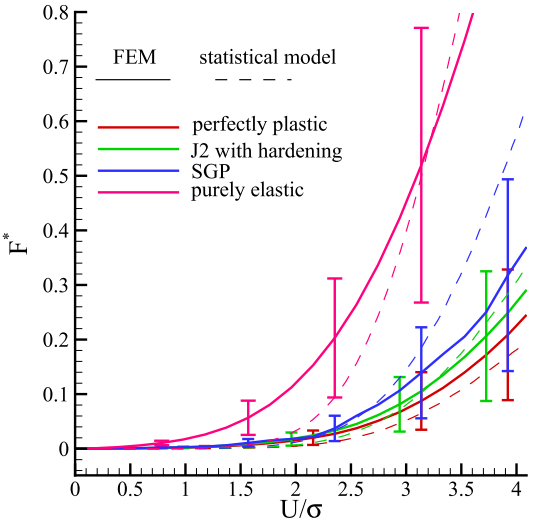

(a)

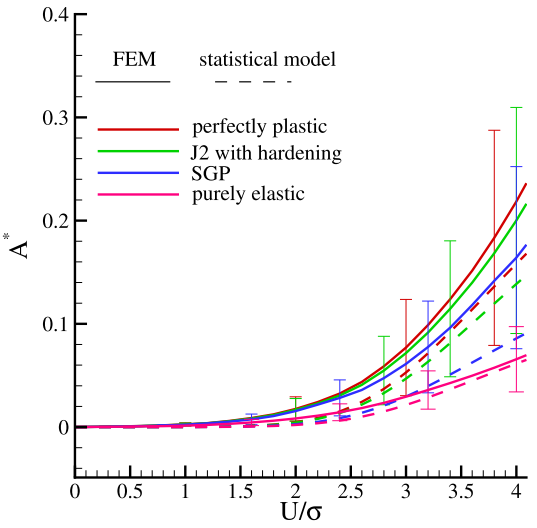

(b)

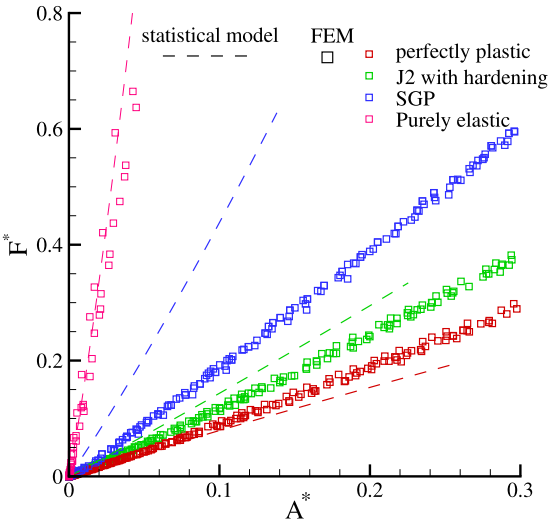

(c)

Fig. 10. Comparison of predictions between FEM model and statistical model for the rough surface with roughness parameters rms = 0.08 μm and l_s = 0.4 μm. (a) Dimensionless force versus interference, (b) dimensionless contact area versus interference, (c) dimensionless force versus dimensionless contact area where the symbols are raw FEM data (the difference in number of data points for different models is a consequence of adaptive loading increment in ABAQUS).

comparison between statistical model predictions with these updated values of R and FEM simulations results are shown in Fig. 12. The other GW parameters (η, σ) have been left unchanged, as it has been shown previously in Vakis (2014) and Song et al. (2014) that the GW model prediction is not very sensitive to these parameters for the values used in this paper. For both roughnesses, a good agreement between statistical model predictions and FEM results is found for contact force versus interference. However, the linear relationship between dimensionless force and area is still quite different for the SGP model, shown in Fig. 12(c). The real average contact pressure, i.e. the slope of the curve, is overestimated in the statistical

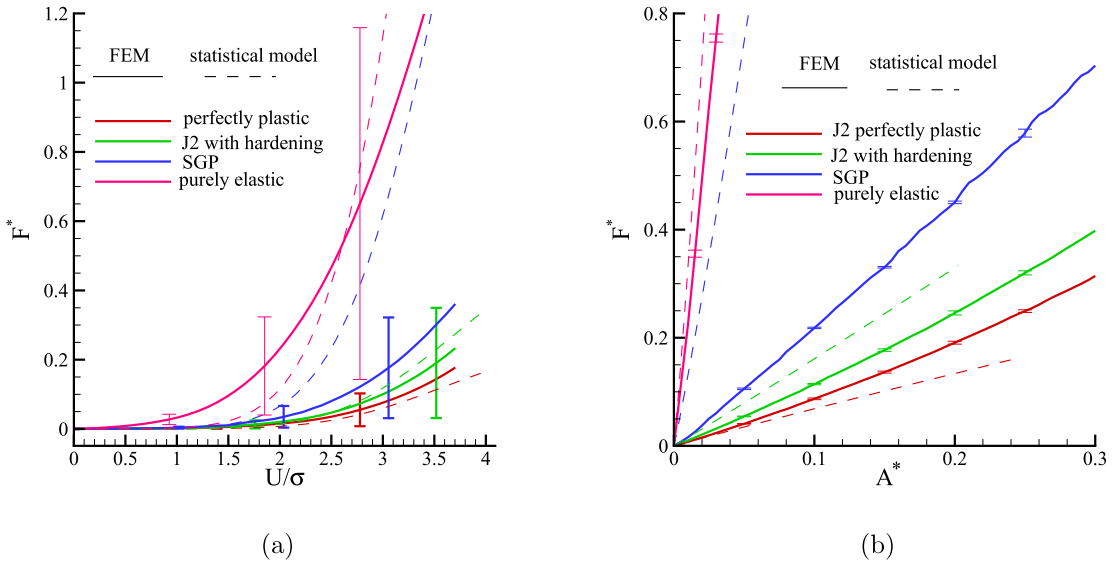

Fig. 11. Comparison of predictions between FEM model and statistical model for the rough surface with roughness parameters rms = 0.16 μm and l_s = 0.4 μm. (a) Dimensionless force versus interference, (b) dimensionless force versus dimensionless contact area.

Table 1
GW parameters for rough surfaces with the same value of $l_s = 0.4$ μm and different rms obtained from Eq. (2).

surface roughness (μm)	R (μm)	η (μm^{-2})	σ (μm)
rms = 0.08	0.36	1.5	0.039
rms = 0.16	0.18	1.5	0.069

model by roughly a factor of two. The results using J_2 plasticity and elasticity also changed somewhat, but within the spread of the five FEM simulations.

6. Discussion and conclusions

The elastoplastic contact of a numerically generated 3D random rough surface was analyzed by both full-detail FEM simulations and a recent modification of the GW model. The GW parameters were extracted through the surface spectral moments of the roughness. The size-dependent elastoplastic behavior of a single asperity contact, which is needed in the statistical analysis, was extracted from strain gradient plasticity simulations. In the spirit of a multiscale approach, the value of the length scale in the strain gradient theory has been fit to 2D simulations of the same asperity problem by means of discrete dislocation plasticity. While varying the asperity size, the fitting is performed for an isolated asperity. Elastic interaction with asperities elsewhere on the rough 3D surface is incorporated by making use of the Hertz solution. The current method does not account for plastic interaction between asperities, since its influence is not significant at the low loads considered here. Recent work in Sun et al. (2015) suggests that elastoplastic interaction is relevant only between small and closely spaced asperities.

In terms of the cost of computational resources and time, the statistical model has a huge advantage over the 3D FEM computations. Yet, it gives qualitatively similar results for the linear dependence between contact (normal) force and contact area, and for the sensitivity of the contact response to surface roughness, material hardening and plastic strain gradient effects.

Quantitatively, the predictions of the statistical model agree with the FEM simulation results for J_2 plasticity (with or without hardening) and pure elasticity when the stochastic variation in surface roughness of finite-size FEM samples is taken into consideration. However, for SGP, the two model predictions for rougher surfaces do not match well, even when taking into account the large stochastic spread in the FEM results. The reason is that for our numerically generated rough surfaces, surface spectral moments underestimate the average radius of curvature R for the GW model. While this underestimation does not have a great impact on the predictions with J_2 plasticity and pure elasticity, it does so for SGP model because of the dependence of the asperity response on R. It is found that by using the classical definition of the radius of curvature

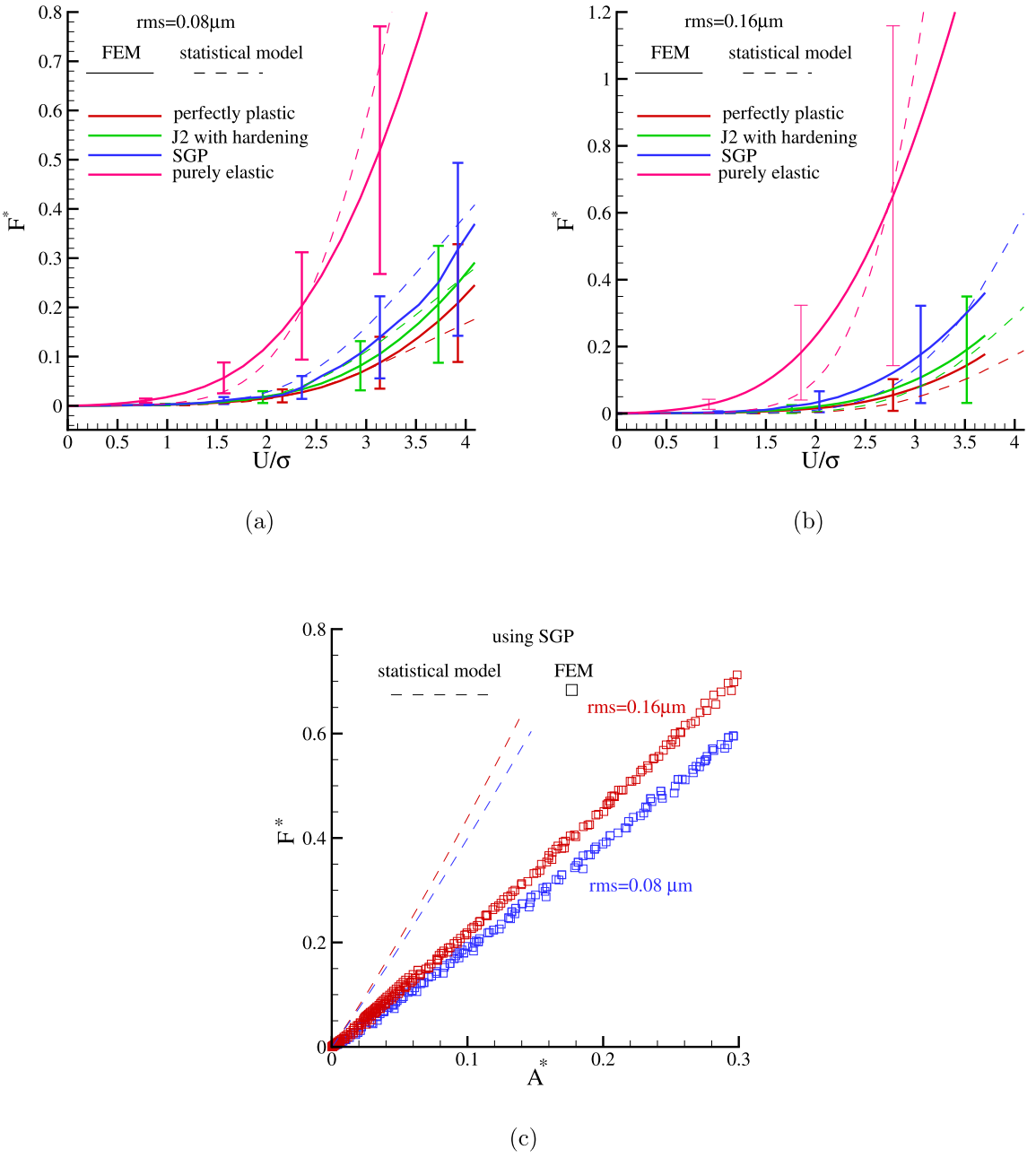

Fig. 12. Comparison between FEM predictions and results of statistical model with R estimated from the numerical surface profile with different roughness parameters. (a) rms = 0.08 μm and $R = 0.5$ μm, (b) rms = 0.16 μm and $R = 0.36$ μm. In all cases, $l_s = 0.4$ μm. (c) Dimensionless force versus dimensionless contact area for statistical and FEM model when using SGP.

of a curve to estimate the average R of all surface asperities, the statistical model gives quantitatively similar results with full-detail FEM simulations for contact force. However, the average contact pressure are still not captured accurately by the statistical model.

To summarize, the salient conclusions of the study are:

- Discrete dislocation plasticity reveals a clear size-dependent behavior of small asperities in contact. When the asperity width w is large enough (for the sample parameters used here, $w > 32$ μm), the behavior becomes size independent. For the same parameter values, the intrinsic length in CMSGP theory is $l = 4.4$ μm.

Table 2
Values of the force–contact area parameter $\kappa = E'\sqrt{2m_2}A/F$ for the various surfaces and materials computed by the statistical model. $E' = E/(1-\nu^2)$ is the plane strain elastic modulus and m_2 the second spectral moment of the surface roughness, cf. Eq. (1).

	rms (μm)	
Material model	0.08	0.16
Elasticity	2.4	2.0
J_2, no hardening	60	113
J_2 with hardening	29	56
CMSGP	11	6.5

Table 3
Fitted values of the parameters in Eq. (8) for the different curves in Fig. 8.

		Perfectly plastic				J2 with hardening			
i		b	m	c	n	b	m	c	n
1	$U/U_c < 1$	1	1.5	1	1	1	1.5	1	1
2	$1 \le U/U_c \le 6$	1	1.518	1	1.137	1	1.533	1	1.124
3	$6 \le U/U_c \le 110$	2	1.195	1	1.135	1.952	1.208	1	1.128
4	$U/U_c > 110$	5.09	1	1.173	1.1	2.562	1.15	1.302	1.07

		SGP $R = 0.36$ μm				SGP $R = 0.18$ μm			
i		b	m	c	n	b	m	c	n
1	$U/U_c < 1$	1	1.5	1	1	1	1.5	1	1
2	$1 \le U/U_c \le 6$	1	1.587	1	1.036	1	1.593	1	1.043
3	$6 \le U/U_c \le 110$	1.5	1.345	1	1.052	1.444	1.397	1	1.033
4	$U/U_c > 110$	2.571	1.227	1.113	1.029	1.442	1.394	0.9558	1.042

		SGP $R = 0.5$ μm			
i		b	m	c	n
1	$U/U_c < 1$	1	1.5	1	1
2	$1 \le U/U_c \le 6$	1	1.578	1	1.048
3	$6 \le U/U_c \le 110$	2.034	1.263	1	1.06
4	$U/U_c > 110$	3.044	1.177	1.12	1.037

- With size-dependent plasticity being incorporated through the CMSGP model, the statistical method is able to predict the dependence of the surface response on the material's plastic properties and on the surface roughness. The contact force in a material exhibiting strain gradient plasticity is significantly larger than in J_2 solid, but at the same time, it is much more sensitive to surface roughness.
- The linear dependence of contact normal force on true contact area persists irrespective of the material's plastic properties and the surface roughness. It is only the value of the force-to-area ratio that depends on the material response, with size dependent plasticity giving a value that approaches the elastic value as the roughness increases. Table 2 summarizes the values found by the statistical model as a function of material behavior and surface roughness.
- When using spectral moments to estimate the average asperity radius curvature R, for moderately rough surfaces (when rms/$l \lesssim 0.02$ for the parameters used here), the statistical predictions of contact force and contact area using strain gradient plasticity agree reasonably well with FEM predictions, but the agreement becomes worse as the surface is rougher. Better agreement is found when using the definition of the radius of curvature to estimate the average R. This also suggests that when size-dependent plasticity is taken into account in the GW statistical model, special attention should be paid on the calculation/measurement of GW roughness parameters, especially for rougher surfaces (smaller R, stronger size dependence). However, even after accurate determination of R, the mean contact pressure is overestimated by the statistical model. Since the strain gradient response of an asperity is sensitive to its size and shape, we attribute this discrepancy to the difference between the shape of the asperities on the numerically generated surface and the hemi-sphere that is input to the statistical model.

Acknowledgments

The work of H.S. was supported by Foundation for Fundamental Research on Matter (FOM), which is part of the Netherlands Organisation for Scientific Research (NWO), grant no. 13POF07-1. The work of X.L. was supported by the National Basic Research Program of China through 2012CB937500, and by the National Natural Science Foundation of China (Grant no. 11202214, no. 91216108, no. 11572329), by State Key Laboratory of Mechanics and Control of Mechanical Structures (NUAA Grant no. MCMS-0114G01), by State Key Laboratory of Structural Analysis for Industrial Equipment (DUT Grant no. GZ15116).

Appendix. Fit parameters as a function of dimensionless interference

Just like in Kogut and Etsion (2002), the flattening response of an individual semi-spherical asperity in terms of flattening force F and contact area A as a function of interference U is fitted by four piecewise power laws of the form

$$F/F_c = b(U/U_c)^m, A/A_c = c(U/U_c)^n,$$

see Eq. (8), where the subscript 'c' denotes the quantities at the onset of plasticity. The values of the fit parameters for each region $i = 1, \ldots, 4$ are given in the following tables, considering three different asperity radii for the SGP results.

References

Bush, A.W., Gibson, R.D., Thomas, T.R., 1975. The elastic contact of a rough surface. Wear 35 (1), 87–111.
Campana, C., Müser, M.H., Robbins, M.O., 2008. Elastic contact between self-affine surfaces: comparison of numerical stress and contact correlation functions with analytic predictions. J. Phys. 20, 354013.
Carbone, G., 2009. A slightly corrected greenwood and williamson model predicts asymptotic linearity between contact area and load. J. Mech. Phys. Solids 57, 1093–1102.
Carbone, G., Bottiglione, F., 2008. Asperity contact theories: do they predict linearity between contact area and load? J. Mech. Phys. Solids 56, 2555–2572.
Chandrasekar, S., Eriten, M., Polycarpou, A.A., 2013. An improved model of asperity interaction in normal contact of rough surfaces. J. Appl. Mech. ASME 80 (1), 011025.
Chang, W.R., Etsion, I., Bogy, D.B., 1987. An elastic-plastic model for the contact of rough surfaces. J. Tribol. ASME 109 (2), 257–263.
Ciavarella, M., Greenwood, J.A., Paggi, M., 2008. Inclusion of 'interaction' in the Greenwood and Williamson contact theory. Wear 265 (5), 729–734.
Cleveringa, H.H.M., Van der Giessen, E., Needleman, A., 1999. A discrete dislocation analysis of bending. Int. J. Plasticity 15 (8), 837–868.
Deshpande, V.S., Needleman, A., Van der Giessen, E., 2005. Plasticity size effects in tension and compression of single crystals. J. Mech. Phys. Solids 53 (12), 2661–2691.
Fleck, N.A., Muller, G.M., Ashby, M.F., Hutchinson, J.W., 1994. Strain gradient plasticity: theory and experiment. Acta Metall. Mater. 42 (2), 475–487.
Fuguo, L., Jinghui, L., Bo, C., Chengpeng, W., Lei, W., 2014. Size effects at dwell stage of micro-indentation for pure aluminum. Rare Metal Mat. Eng. 43 (12), 2931–2936.
Van der Giessen, E., Needleman, A., 1995. Discrete dislocation plasticity: a simple planar model. Model. Simul. Mater. Sci. Eng. 3 (5), 689.
Greenwood, J.A., 2006. A simplified elliptic model of rough surface contact. Wear 261 (2), 191–200.
Greenwood, J.A., Williamson, J.B.P., 1966. Contact of nominally flat surfaces. Proc. R. Soc. Lond. A 295, 300–319.
Huang, Y., Qu, S., Hwang, K.C., Li, M., Gao, H., 2003. A conventional theory of mechanism-based strain gradient plasticity. Int. J. Plasticity 20, 753–782.
Jackson, R.L., 2006. The effect of scale-dependent hardness on elasto-plastic asperity contact between rough surfaces. Tribol. Trans. 49 (2), 135–150.
Kalin, M., Pogacnik, A., Etsion, I., Raeymaekers, B., 2016. Comparing surface topography parameters of rough surfaces obtained with spectral moments and deterministic methods. Tribo. Inter. 93, 137–141.
Kogut, L., Etsion, I., 2002. Elastic-plastic contact analysis of a sphere and a rigid flat. J. Appl. Mech. ASME 69 (5), 657–662.
Li, H., Torrance, K.E., 2005. An experimental study of the correlation between surface roughness and light scattering for rough metallic surfaces. SPIE Conf. Adv. Character. Technol. Opt. Semicond. Nanotechnol. II 5878, 1–15.
McCool, J.I., 1986. Comparison of models for the contact of rough surfaces. Wear 107 (1), 37–60.
McCool, J.I., 1987. Relating profile instrument measurements to the functional performance of rough surfaces. J. Tribol. ASME 109 (2), 264–270.
Nix, W.D., Gao, H., 1998a. Indentation size effects in crystalline materials: a law for strain gradient plasticity. J. Mech. Phys. Solids 46 (3), 411–425.
Nix, W.D., Gao, H., 1998b. Indentation size effects in crystalline materials: a law for strain gradient plasticity. J. Mech. Phys. Solids 46 (3), 411–425.
Pawlus, P., Zelasko, W., Michalski, J., 2012. Surface topography parameters important in contact mechanics. J. Auto. Mob. Rob. Intel. Systems 6, 16–19.
Pei, L., Hyun, S., Molinari, J.F., Robbins, M.O., 2005. Finite element modeling of elasto-plastic contact between rough surfaces. J. Mech. Phys. Solids 53 (11), 2385–2409.
Persson, B.N.J., 2001. Theory of rubber friction and contact mechanics. J. Chem. Phys 115, 3840–3861.
Qu, S., Huang, Y., Nix, W.D., Jiang, H., Zhang, F., Hwang, K.C., 2004. Indenter tip radius effect on the NixGao relation in micro-and nanoindentation hardness experiments. J. Mater. Res. 19 (11), 3423–3434.
Song, H., Dikken, R.J., Nicola, L., Van der Giessen, E., 2015. Plastic ploughing of a sinusoidal asperity on a rough surface. J. Appl. Mech. ASME 82 (7), 071006.
Song, H., Van der Giessen, E., Liu, X., 2016. Strain gradient plasticity analysis of elasto-plastic contact between rough surfaces. J. Mech. Phys. Solids 96, 18–28.
Song, H., van der Giessen, E., Vakis, A.I., 2014. Erratum: asperity interaction and substrate deformation in statistical summation models of contact between rough surfaces. Appl. Mech. ASME 81 (4), 041012.
Sun, F., Van der Giessen, E., Nicola, L., 2012. Plastic flattening of a sinusoidal metal surface: a discrete dislocation plasticity study. Wear 296 (1), 672–680.
Sun, F., Van der Giessen, E., Nicola, L., 2015. Interaction between neighboring asperities during flattening: a discrete dislocation plasticity analysis. Mech. Mater. 90, 157–165.
Tabor, D., 2000. The Hardness of Metals. Oxford University Press.
Vakis, A.I., 2014. Asperity interaction and substrate deformation in statistical summation models of contact between rough surfaces. J. Appl. Mech. ASME 81 (4), 041012.
Widjaja, A., Van der Giessen, E., Needleman, A., 2005. Discrete dislocation modelling of submicron indentation. Mater. Sci. Eng. A 400, 456–459.
Xue, Z., Huang, Y., Li, M., 2002. Particle size effect in metallic materials: a study by the theory of mechanism-based strain gradient plasticity. Acta Mater. 50 (1), 149–160.
Yu, N., Polycarpou, A.A., 2004. Extracting summit roughness parameters from random gaussian surfaces accounting for asymmetry of the summit heights. In: ASME/STLE 2004 Inter. Joint Tribol. Conference, pp. 1209–1215.
Zhang, F., Huang, Y., Hwang, K.C., 2006. The indenter tip radius effect in micro-and nanoindentation hardness experiments. Acta Mech. Sinica 22 (1), 1–8.